Journal of Solid and Fluid Mechanics (JSFM), 15(5): 23-27, 2025

Shahrood University of Technology

Journal of Solid and Fluid Mechanics (JSFM)

DOI: 10.22044/jsfm.2025.16493.3991

Manufacturing Engineering of Iran

Effect of Travel Speed on CK45 Steel Welding: A Comprehensive Analysis of Mechanical Properties, Corrosion Behavior, Energy Input, and Processing Time

Sayyed Mohammadreza Sedehi[1], Alireza Araee[2,*], Masoud Jafarpour[3], Raha Molavi dosangani[4], Alisina Mortezaei Moghadam[5]

[1] Ph.D. Student, Mech. Eng., Tehran Univ., Tehran, Iran.
[2] Assoc. Prof., Mech. Eng., Tehran Univ., Tehran, Iran.
[3] M.Sc. graduate., Materials. Eng., Sirjan Azad Univ., Sirjan, Iran.
[3] Ph.D. Student., Mech. Eng., Guilan Univ., Guilan, Iran.
[4] B.E.E. Student., Mech. Eng., Isfahan Univ of Technology., Isfahan, Iran.

*Corresponding author: alaraee@ut.ac.ir
Received: 07/12/2025 Revised: 09/24/2025 Accepted: 10/29/2025

Abstract

This study investigates the effect of hand travel speed in manual arc welding using E6013 electrodes on the microstructural, mechanical, and corrosion properties of welds on CK45 steel. Welding was performed at five different speeds (17, 20, 26, 32, and 39 cm/min) in the flat position. Various tests, including Vickers hardness, potentiodynamic corrosion, XRD analysis (for crystallite size and microstrain), and OCP analysis were conducted. The results indicated that the 26 cm/min speed yielded the best overall performance, with the lowest microstrain (0.0021), smallest crystallite size (68 nm), and highest hardness (265 HV). Although the corrosion rate was moderate at this speed (0.0079 mm/year), structural stability and uniform phase distribution were evident. The highest corrosion rate occurred at 17 cm/min (0.022 mm/year), and the lowest at 39 cm/min (0.021 mm/year), though the latter showed the lowest hardness (186 HV). From a practical standpoint, welding at the intermediate speed offered optimal performance in terms of time, energy consumption, and defect minimization. This study highlights the critical role of travel speed in achieving a balance between mechanical performance, corrosion resistance, and process efficiency in manual welding.

Keywords Welding, CK45 steel, speed, corrosion.

1. Introduction

Welding is regarded as one of the most vital and widely used manufacturing processes across various industries, enabling the creation of permanent, strong, and efficient joints between metallic—and occasionally non-metallic components [1,2]. This process plays a key role in the fabrication of heavy structures [3], pipelines [4], power plant equipment [5], industrial machinery, and even emerging fields such as robotics and medical device manufacturing [6,7].

Beyond the technical aspects, hand movement speed has a significant influence on the total operation time, welding energy consumption, and consequently, the final production cost [8]. Two critical parameters for evaluating the final weld quality are surface hardness and corrosion resistance, both of which are directly related to component performance and service life [9]. Nevertheless, no prior research has simultaneously investigated the influence of the welder's hand speed on mechanical properties, corrosion behavior, operational time, and process cost in an integrated manner or such studies have not been systematically documented. This research gap, particularly for widely used carbon steels such as CK45, provides a valuable opportunity to generate innovative and applicable knowledge. The present study, focusing on the role of the welder's hand speed in the manual welding of CK45 steel, introduces a multidisciplinary and innovative approach in which a set of technical and economic indicators are evaluated concurrently.

2. Materials and Experiments

In this study, 4-mm-thick CK45 carbon steel sheets and 2.5-mm-diameter E6013 covered manual electrodes were used, with their chemical compositions presented in Tables 1 and 2. CK45 steel, due to its balanced content of carbon, manganese, and minor alloying elements, exhibits moderate hardness, suitable heat-treatability, and adequate mechanical strength for industrial welding applications.

The welding process was carried out using 2.5-mm-diameter E6013 covered electrodes, following the schematic illustrated in Figure 1. This type of electrode is highly suitable for medium-thickness sheets because it provides a stable arc, good surface adhesion, and produces a smooth and uniform weld. The electrodes were dried for 3 hours at 260 °C to prevent moisture absorption and avoid

porosity formation in the weld seam [10]. Initially, CK45 steel sheets were cut to the required dimensions for various tests. After cutting, all surfaces designated for testing were cleaned using a wire brush, fine sandpaper, and acetone solvent to remove surface contaminants, iron oxides, and rust. Welding of the samples was performed manually in a flat position. An experienced operator executed the weld beads while maintaining constant current, voltage, and electrode type, but the hand travel speed along the weld line was varied. Different hand speeds were determined and applied based on the welding time per unit length, as detailed in Table 3. These speeds were set at three levels: low, medium, and high, to create a diverse range of welding conditions. For precise measurement of the welder's hand speed, a marking system and graduated rulers were placed alongside the workpiece, allowing calculation of the average hand speed based on the time required to weld a specified length. Potential sources of error, such as minor variations in hand movement rhythm, were also considered. In all samples, the welding machine output current was set between 100–110 A with an operating voltage of approximately 22 V. Welding current and voltage were monitored and maintained within a fixed range throughout all experiments.

Fig.1 – Schematic of the Welding Process

3. Discussion and Conclusion

XRD Analysis

XRD analysis was conducted on the welded samples to identify the phases formed in the weld zone and to extract microstrain and crystallite size. The results for the produced samples are shown in Fig.2. The XRD patterns for the five samples welded at different hand speeds indicate that there are no shifts in the positions of the main peaks. The tallest peak occurs at 45°, typically corresponding to the dominant ferrite phase ($Fe_{2-3}N$) in plain carbon steels such as CK45 [11]. Additionally, weaker peaks at 65° and 85° confirm the presence of polyhedral ferritic grains and possibly a minor γ′-phase (Fe_4N) in the base structure. The 45° peak also reflects the preferential crystallographic orientation. Minor variations in its intensity between samples can be attributed to slight changes in grain size or residual stresses resulting from different heat transfer rates [12]. Overall, the phase stability observed in the XRD results can be interpreted as a positive indicator of metallurgical stability in the weld zone when using E6013 electrodes, particularly under carefully controlled welding parameters [13]. Crystallite sizes, calculated from the XRD peaks using the Scherrer equation, ranged from 270 nm in the first sample down to 68 nm in the third sample, and then increased to 163 nm in the fifth sample. In the third sample, which corresponds to the optimal hand speed (26 cm/min), the smallest crystallite size was obtained, reflecting an optimized microstructure with refined grains and, consequently, improved mechanical properties such as increased hardness and strength. The reduction in crystallite size to this level is generally attributed to a uniform and controlled cooling rate in the weld zone [14]. Microstrain values were distributed nonlinearly among the samples. In the first sample (low hand speed), the microstrain was 0.003, decreasing to 0.0021 in the third sample. In the fourth and fifth samples, a mild increase in microstrain was observed, likely due to very rapid cooling, heterogeneous solidification, or fluctuations in the molten pool [15].

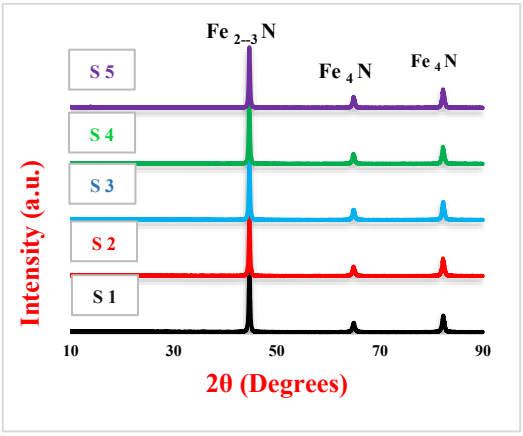

Fig.2 – XRD Results of the Welded Samples

The variations in microhardness in the presence of different reinforcing factors are shown in Figure 3. The assigned hardness values indicate that the third sample, welded at a hand speed of 26 cm/min, exhibits the highest hardness (265 HV). In this sample, the crystallite size reached its minimum value (68 nm), and the microstrain was also at its lowest (0.0021). These two factors indicate the formation of a uniform, fine, and dense grain structure in the weld zone, which aligns well with the expected microstructural principles of materials. According to the Hall-Petch relationship,

grain size reduction directly increases hardness because grain boundaries act as barriers to dislocation motion, thereby enhancing the plastic resistance of the material [16]. Conversely, the first sample, which had the largest grain size (270 nm) and the highest microstrain (0.003), exhibited the lowest hardness (186 HV). The elevated microstrain indicates higher internal stresses and possibly crystal defects, which reduce structural cohesion and result in diminished mechanical properties. Intermediate samples, numbers 2 and 4, with moderate grain sizes and microstrains, exhibited hardness values between these two extremes. Therefore, this analysis demonstrates that properly adjusting the welder's hand speed directly influences crystallite size and ultimately the final weld hardness. The lower hardness observed in sample S4, despite its small crystallite size, can be attributed to lower residual stresses and also to the inverse interpretation of the Hall-Petch relationship [17].

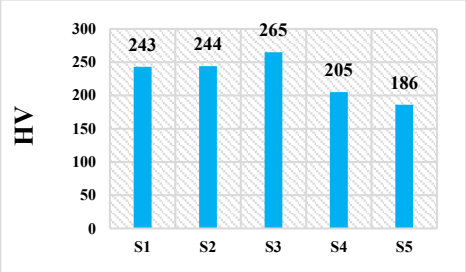

Fig. 3 – Vickers Microhardness Results of the Produced Samples

Potentiodynamic Polarization Corrosion Test

Based on data derived from the Stern-Geary equation [18], a decrease in corrosion potential indicates a lower thermodynamic tendency for corrosion in these samples [19]. The lowest corrosion rate was observed in the fifth sample, at 0.0021 mm/year, corresponding to a hand speed of 39 cm/min. In this sample, although the crystallite size is relatively large (163 nm), the microstrain remains at a moderate level (0.0025), which may indicate a stable, low-stress structure [20]. Additionally, the increased hand speed in this sample may have reduced the effective heat-affected zone, leading to the formation of more uniform oxide layers and improved corrosion resistance. In contrast, the first sample exhibited the highest susceptibility to corrosion, with a corrosion rate of 0.022 mm/year. Its high microstrain and large grain size suggest a less stable, more stressed structure, promoting internal stress concentration, weakening the oxide layer, and facilitating electrochemical attack [21]. Overall, it can be concluded that, unlike hardness which is primarily influenced by grain refinement—the corrosion rate is more dependent on residual stresses and the uniformity of the surface structure [22,23]. Sample three, which exhibits high hardness but a moderate corrosion rate, illustrates that an inherent balance is required between mechanical strength and corrosion resistance.

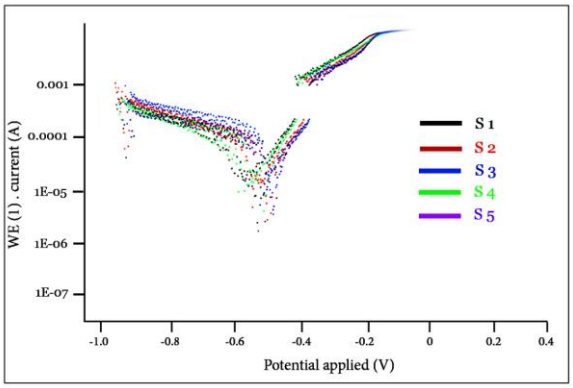

Fig.4 – Corrosion Test Results of the Produced Samples

Analysis of Energy Consumption, Welding Time, and Engineering Economics

In manual electrode welding, one of the key factors affecting energy consumption and economic efficiency is the operator's hand travel speed, which directly influences welding time, electrode consumption, heat losses, and the uniformity of heat transfer [24]. Process efficiency values for welding are generally based on older references [25–28] or applicable welding standards. These standards [29,30] typically provide only general efficiency values for various welding processes without differentiating adjustable process conditions. The heat input can be calculated using Equation (1) [31]:

$$Q=P\_w/v\_w \times \eta$$

where Qis the heat input per unit length (kJ/mm), P_w is the welding power (W), v_wis the welding speed (mm/s), and ηis the welding process efficiency. The heat input depends not only on the process efficiency but also on the welding power and speed. From Equation (1), it is clear that for constant welding power (P_w) and process efficiency (η), the heat input is inversely proportional to the welding speed ($1/v\_w \propto Q$). Therefore, if the welding speed decreases, Qper unit length increases (e.g., halving v_w doubles Q), and conversely, increasing the welding speed reduces the heat input per unit length. Practically, variations in Qhave significant effects on thermal distribution and consequences: low speeds result in higher heat input per unit length, longer thermal cycles, a wider heat-affected zone (HAZ), deeper penetration, slower cooling rates, higher probability of distortion and residual stresses, and grain growth due to prolonged exposure at elevated temperatures. In contrast, higher speeds lead to lower heat input per unit length, narrower HAZ, reduced penetration (risking lack of fusion or incomplete penetration), faster cooling rates that may produce harder but more brittle microstructures, reduced distortion, and an increased likelihood of weld heterogeneity (e.g., localized incomplete fusion). It is important to note that although the instantaneous power transferred from the source (P_w) is constant in both cases, the fundamental

difference lies in its distribution over the welded length: at low speeds, more energy is delivered per millimeter, whereas at high speeds, the same energy is distributed over a greater length. Therefore, to control the mechanical properties and microstructure of the welded component, welding speed must be carefully coordinated with power selection and other parameters (e.g., preheating, controlled cooling, or multi-pass welding) to maintain the heat input (Q) within an optimal range for achieving the desired properties. At speeds below the optimal level, such as 17 cm/min, the process time increases, resulting in higher energy consumption, greater risk of edge burn, and prolonged current usage.

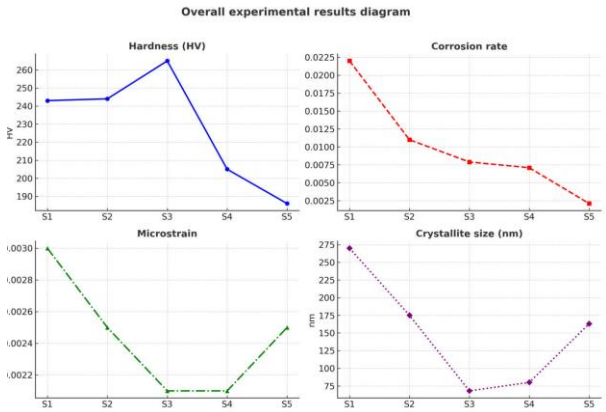

Fig.6 – Overall Relationships Among the Results

4. Conclusion

1. Mechanical Properties: The sample welded at a hand speed of 26 cm/min (sample 3) exhibited the highest hardness and the finest crystallite size, indicating a homogeneous structure and high resistance to deformation.
2. Corrosion Resistance: The same sample demonstrated the lowest corrosion rate and stable microstrain, consistent with OCP test results. This suggests that the stability of the electrochemical potential and the successful formation of a passive layer can be directly attributed to precise control of welding speed.
3. Economic Efficiency: The optimal sample not only required the least energy and welding time for a standard weld but also minimized the need for rework or post-weld repairs.
4. Effects of Non-Optimal Speeds: Hand speeds outside the optimal range whether lower or higher resulted in decreased hardness, increased corrosion rate, reduced structural quality, and higher costs due to energy waste and additional rework.
5. Overall Implication: Precise control of hand speed in manual welding is not only a qualitative factor affecting weld quality but also a key parameter in ensuring component longevity and reducing maintenance costs.

5. References

[1] Soto-Diaz R, Vasquez-Carbonell M, Escorcia-Gutierrez J. A review of artificial intelligence techniques for optimizing friction stir welding processes and predicting mechanical properties. *Engineering Science and Technology, an International Journal*. 2025 Feb 1;62:101949.

[2] Wang PE, Ghassemi-Armaki H, Pour M, Zhao X, Ma J, Sattari K, Carlson B. Applicable and generalizable machine learning for intelligent welding in automotive manufacturing. *Welding in the World*. 2025 Feb 7:1-36.

[3] da Silva Machado T, Machado IG. Structural Impact on High-Strength Low-Alloy Steel Structures Welded by Gas Metal Arc Welding with Nickel and Steel Filler Metals. *Journal of Materials Engineering and Performance*. 2025 May 9:1-4.

[4] Zhu C, Wang Z, Zhu Z, Guo J. Design and modeling of pipeline welding robot based on Pieper criterion and construction of integrated intelligent welding system. *Welding in the World*. 2025 Jul 7:1-5.

[5] Duhanets V, Semenyshena R, Fedirko P, Pukas V, Volynkin M. Application of automated welding processes in the restoration of pipelines of power facilities. Machinery & Energetics. 2025 Jan 1;16(1).

[6] Kuo CC, Chen HW, Farooqui A, Huang SH, Tseng SF. Enhancing the mechanical integrity of Polylactic acid components via ultrasound-assisted rotary friction welding for sustainable medical device fabrication. *Journal of Manufacturing Processes*. 2025 May 15;141:1324-36.

[7] Bhattacharjee J, Roy S. Welding Automation and Robotics. Advanced Welding Technologies. 2025 May 5:47-71.

[8] Jármai K, Farkas J (1999) Cost calculation and optimisation of welded steel structures. *Journal of Constructional Steel Research*. 1;50(2):115-35.

[9] Li S, Hou X, Wang X, Liu Z, Xia Y, Dong H (2023) Weldability of high entropy alloys: microstructure, mechanical property, and corrosion resistance. *Journal of Manufacturing Processes*. 4;99:209-29.

[10] Junaidi A, Wilza R, Hendradinata H (2024) Analysis of Variation E7016 Electrode Heating Time and Humidity on E7016 Electrode Tensile Strength of Joints Welding Material SS400. International *Journal of Mechanics, Energy Engineering and Applied Science* (IJMEAS). 30;2(3):48-53.

[11] Sedehi SM, Yazdi SH, Bazleh Z, Boskabadi M, Sistani A (2024) Fabrication of CK45/RGO Nanocomposite Using Machining Chips Recycling and Spark Plasma Sintering. International *Journal of Iron & Steel Society of Iran*. 21;20(2):73-80.

[12] Sedehi, Khosravi, Yaghoubinejad (2024) An experimental comparison of the microstructure and surface properties of Al/Al_2O_3 samples produced by powder metallurgy and spark plasma sintering methods. *Mechanics of Structures and Fluids*. 22;12(5):123–132.

[13] Abderrahmani S, Chérifi N, Ghanem K (2024) Study of the effect of SMAW welding speed on the microstructure and crystal stability of X70 steel using X-ray diffraction. *Studies in Engineering and Exact Sciences*. 24;5(2):e9691-.

[14] Singh VP, Kumar D, Kuriachen B (2024) Parametric effect on microstructure evolution, grain size and mechanical behaviour of friction stir butt welding of AA6061-T6 alloy. *Journal of Adhesion Science and Technology*. 18:1-25.

[15] Jia L, Cui H, Yang S, Lv S, Xie X, Qu J (2024) Effect of the cooling rates on the microstructure and segregation characteristics in directionally solidified GH4151 superalloy. Materials Characterization 1;209:113735.

[16] Sedehi SM, Khosravi M, Yaghoubinezhad Y (2021) Mechanical properties and microstructures of reduced graphene oxide reinforced titanium matrix composites produced by spark plasma sintering and simple shear extrusion. *Ceramics International*. 1;47(23):33180-90.

[17] Aftab M, Aftab A, Butt MZ, Ali D, Bashir F, Iqbal SS. Surface hardness of pristine and laser-treated zinc as a function of indentation load and its correlation with crystallite size valued by Williamson-Hall analysis, size-strain plot, Halder-Wagner and Wagner-Aqua models. *Materials Chemistry and Physics*. 2023 Feb 1;295:127117.

[18] Cheng L, Liu C, Han D, Ma S, Guo W, Cai H, et al (2019) Effect of graphene on corrosion resistance of waterborne inorganic zinc-rich coatings. *J Alloys Compd* ;774: 255–64

[19] Taheridoustabad, Iman, Mohammad Khosravi, and Yadollah Yaghoubinezhad (2021) "Fabrication of GO/RGO/TiC/TiB2 nanocomposite coating on Ti–6Al–4V alloy using electrical discharge coating and exploring its tribological properties." *Tribology International* 156 (2021): 106860.

[20] Abdel-Rahman AS, Sabry YA (2024) An approach to the micro-strain distribution inside nanoparticle structure. International *Journal of Non-Linear Mechanics*. 1;161:104670.

[21] Konar R, Maiti S, Shpigel N, Aurbach D (2023) Reviewing failure mechanisms and modification strategies in stabilizing high-voltage LiCoO2 cathodes beyond 4.55 V. *Energy Storage Materials*. 1;63:103001.

[22] Shirazi H, Wang S, Chen W, Eadie R (2024) Pipeline circumferential corrosion fatigue failure under the influence of bending residual stress in the near-neutral pH environment. *Engineering Failure Analysis*. 1;166:108887.

[23] Akinwamide SO, Venter A, Akinribide OJ, Babalola BJ, Andrews A, Olubambi PA (2022) Residual stress impact on corrosion behaviour of hot and cold worked 2205 duplex stainless steel: A study by X-ray diffraction analysis. Engineering Failure Analysis. 1;131:105913.

[24] Tadjikuziev R, Rubidinov S, Mamatqulova S (2024) Advancements in energy-efficient welding production techniques: Innovative models and methods for combined workpiece fabrication. InE3S Web of Conferences (Vol. 583, p. 05005). EDP Sciences.

[25] Pepe N, Yapp D (2008) Measurements of process efficiency for a range of MIG/MAG welding process. In: 17th International Conference Computer *Technology in Welding and Manufacturing*, Cranfield, GB, pp 1–11, ISBN 978-1-903761-07-6 .

[26] Shinoda T, Hayashi C, Kato Y (2001) Directed plasma fabrication. In: *Proceedings of the International Conference of Materials*, Helsingor, DK, TIB-RN9585(10), BAM-DS-Proc.13-D076/02, pp 258–267 .

[27] DuPont JN, Marder AR (1995) Thermal efficiency of arc welding processes. *Weld J* 74:406–416, ISSN 0043-2296.

[28] Giedt WH, Tallerico LN, Fuerschbach PW (1989) GTA welding efficiency: calorimetric and temperature field measurements. *Weld J* 68:28–32, ISSN 0043-2296.

[29] DIN EN 1011-1 (2009) Welding—recommendations for welding of metallic materials–part 1: General guidance for arc welding; German version EN 1011-1

[30] SEW 088 (1993) supplemental sheet 2 BWeldable fine grained steels; guidelines for processing, particular for fusion welding.

[31] Haelsig A, Mayr P, Kusch M. Determination of energy flows for welding processes. *Welding in the World*. 2016 Mar;60(2):259-66.